A composite cavity model for axisymmetric high Reynolds number separated flow II: Numerical analysis and results*

A.D. FITT[1] and P. WILMOTT[2]

[1]*Faculty of Mathematical Studies, University of Southampton SO9 5NH, U.K.*
[2]*Mathematical Institute, 24–29 St. Giles, Oxford OX1 3LB, UK and Department of Mathematics, Imperial College, London SW7 2BZ, U.K.*

Abstract. In a companion paper (Wilmott and Fitt (1992)) a model was proposed for the separated high Reynolds number flow past a three-dimensional slender axisymmetric body. This 'composite' model assumes that downstream of the body there is both a region of constant pressure and a Prandtl – Batchelor region. Matched asymptotic expansions were employed to recover a non-linear integro-differential equation for the shape of the separated region and some asymptotic solutions were obtained. The present study concerns the numerical solution of this equation and more detailed results concerning the cavity shape and closure properties.

1. Introduction

In Wilmott and Fitt (1992) a 'composite' model was proposed for the high Reynolds number flow past an axisymmetric three-dimensional body. This model may be thought of as a combination of the classical constant pressure Helmholtz–Kirchhoff model and the constant vorticity Prandtl–Batchelor model (see, e.g. Childress, 1966). In spite of the simplicity and elegance of these models, it has long been known that, if either model is used alone to try to describe separated flows, each suffers from the drawback that they display poor agreement with experiment. For two-dimensional flow, much better agreement with experiment was obtained by the composite model of O'Malley et al. (1991) where the separated region was assumed to consist of a constant-pressure region followed by a region of (unknown) constant vorticity. In the two-dimensional case, the entire problem may be reduced to a single nonlinear singular integro-differential equation (NLSIDE) with a Cauchy kernel that must be solved in order to determine the shape of the dividing streamline. Although the solution of such equations is far from a trivial matter, effective numerical procedures have been developed (see also Fitt et al., 1985) that allow the problem to be solved with accuracy and economy. The current study focuses on the axisymmetric case, where the numerical solution of the relevant NLSIDEs presents a much more formidable challenge. In the next section some of the difficulties involved are discussed and the (very few) previous attempts to solve similar problems are reviewed.

A schematic diagram of the flow appears in Fig. 1. The slender axisymmetric body is assumed to have a radius H_1 and the cavity reattaches smoothly to an afterbody of radius H_2. The region R_{i1} (length L) is one of constant pressure, whilst the region R_{i2} (length
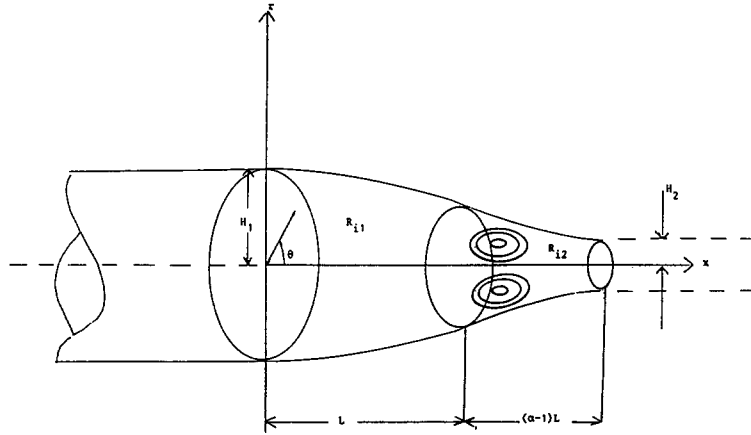
Fig. 1. Definition sketch showing the separating stream surface, stagnant zone R_{i1}, Prandtl–Batchelor region R_{i2} and equivalent afterbody.

$(\alpha - 1)L)$ is a Hill's vortex (see Hill, 1894). This is the axisymmetric analogy of a Prandtl–Batchelor region of constant vorticity in two-dimensional flow, and, according to a classical result of Batchelor (1955) the vorticity therein is proportional to the radial distance r.

In Section 2 below the flow model is summarized and possible numerical approaches are discussed. The numerical method that was used in this study is explained in Section 3, whilst Section 4 contains numerical results of both test cases and real computations. Some conclusions concerning the model and the numerical solution of such equations are drawn in Section 5.

2. The composite axisymmetric cavity equation

In Wilmott and Fitt (1992) matched asymptotic expansions were employed to determine the equation satisfied by the cavity boundary. The small parameter in the problem was given by ϵ, which was itself defined by

$$\epsilon^2 = \frac{p_\infty - p_c}{\frac{1}{2}\rho U_\infty^2}.$$

Here p_∞ denotes the pressure far away from the axisymmetric body, p_c is the pressure in the cavity R_{i1}, whilst ρ and U_∞ are respectively the free stream density and velocity; ϵ is small because the body is slender. Denoting the cavity boundary by $r^* = R^*(x^*)$, where the star indicates that lengths have been non-dimensionalized with ϵ, it was shown that R^* satisfies the NLSIDE

$$\frac{d}{dx}\left[\frac{1}{2}R^*R^{*\prime}\log\left(\frac{\epsilon^2}{4x(\alpha - x)}\right) - \frac{1}{2}\int_0^\alpha \frac{R^*(\xi)R^{*\prime}(\xi) - R^*(x)R^{*\prime}(x)}{|x - \xi|}d\xi\right]$$

$$= -\frac{1}{2}R^{*\prime 2} - (R^*R^{*\prime})'\log R^* + \begin{cases} 1/2 & (0 \leq x \leq 1) \\ \frac{h^*}{2} + \beta^{*2}R^{*4}/32 & (1 \leq x \leq \alpha). \end{cases} \quad (1)$$

Here derivatives are denoted by a prime, h^* is the scaled jump in the Bernoulli constant across the dividing separating streamline and β^* is the scaled vorticity in region R_{i2}. The interested reader is referred to Wilmott and Fitt (1992) for the details of (1) and the scalings. (Note that Wilmott and Fitt (1992) contains some minor typographical errors.)

For both analytical and numerical purposes (1) is somewhat inconvenient, and it proves significantly simpler to work in terms of the cavity area rather than the radius. Setting

$$T(x) = \pi R^{*2}(x)$$

and dropping the stars for convenience, the equation becomes

$$\frac{\mathrm{d}}{\mathrm{d}x}\left[T'(x)[\log(\epsilon/2) - \log\sqrt{x(\alpha - x)}] - \frac{1}{2}\int_0^\alpha \frac{T'(\xi) - T'(x)}{|x - \xi|}\,\mathrm{d}\xi \right]$$
$$+ \frac{T'^2(x)}{4T(x)} + \frac{T''(x)}{2}\log\left(\frac{T}{\pi}\right) = \begin{cases} \pi & (0 \leqslant x \leqslant 1) \\ \pi h + \beta^2 T^2(x)/16\pi & (1 \leqslant x \leqslant \alpha) \end{cases}. \tag{2}$$

Continuity of pressure at $x = 1$ requires that

$$h = 1 - \frac{\beta^2 T^2(1)}{16\pi^2},$$

and the boundary conditions are

$$T(0) = \frac{\pi H_1^2}{\epsilon^2 L^2}, \qquad T(\alpha) = \frac{\pi H_2^2}{\epsilon^2 L^2},$$

and (assuming smooth separation and reattachment)

$$T'(0) = T'(\alpha) = 0.$$

As far as numerical calculations are concerned, it transpires that for practical purposes it is best to perform some preliminary simplification on (2). Splitting the integral term into two portions, integrating by parts and differentiating, we find that the equation may be written

$$-\frac{1}{2}\int_0^\alpha \frac{T''(\xi) - T''(x)}{|\xi - x|}\,\mathrm{d}\xi + \frac{T''(x)}{2}\log\left[\frac{\epsilon^2 T(x)}{4\pi x(\alpha - x)}\right]$$
$$+ \frac{T'^2(x)}{4T(x)} = \begin{cases} \pi & (0 \leqslant x \leqslant 1) \\ \pi - \beta^2[T^2(1) - T^2(x)]/16\pi & (1 \leqslant x \leqslant \alpha) \end{cases}$$

with

$$T(0) = \frac{\pi H_1^2}{\epsilon^2 L^2}, \qquad T(\alpha) = \frac{\pi H_2^2}{\epsilon^2 L^2}, \qquad T'(0) = T'(\alpha) = 0. \tag{3}$$

The equation may also be expressed in other forms, but we proceed henceforth using (3).

In Wilmott and Fitt (1992) there was a discussion of the relationship between the boundary conditions and the requirement of cusped closure. Provided that both H_1 and H_2 exceed zero, cusped closure, and hence finiteness of pressure, is ensured by $T'(0) = T'(\alpha) = 0$. An asymptotic analysis given in Wilmott and Fitt (1992) showed that under these

conditions, it follows that $T''(0) = T''(\alpha) = 0$. A result of the discussion contained therein is that, in the case when $H_2 = 0$ and therefore $T(\alpha) = 0$ it would be possible to improve the model by employing a more sophisticated slender body theory.

2.1. Consistency conditions for the equation and discussion

Before discussing possible numerical strategies for the solution of (3), we note the important result that not all of the parameters in (3) are independent. This fact has been noted before for two-dimensional models by Childress (1966), who derived relationships by what amounted essentially to a global force balance, and by O'Malley et al. (1991) using a simpler argument. A similar analysis is applicable in the present case. Multiplying equation (3) through by $T'(x)$ and integrating from 0 to α with respect to x allows the whole of the right-hand side and much of the left-hand side of the equation to be integrated immediately, giving

$$\frac{1}{2}\int_0^\alpha \left[T''(x)\, T'(x) \log(x(\alpha - x)) + T'(x)\left(\int_0^\alpha \frac{T''(\xi) - T''(x)}{|\xi - x|}\, d\xi\right)\right] dx = \pi(T(\alpha) - T(0))$$

$$- \frac{\beta^2}{16\pi}\left(T^2(1)T(\alpha) - \frac{T^3(\alpha)}{3} - \frac{2T^2(1)}{3}\right).$$

An integration by parts shows that the left-hand side is identically zero, so that

$$\beta^2 = \frac{16\pi^2(T(\alpha) - T(0))}{T^2(1)T(\alpha) - \dfrac{T^3(\alpha)}{3} - \dfrac{2T^3(1)}{3}}. \tag{4}$$

This result effectively relates the vortex strength to the height of the obstacle and the length of the constant pressure region; numerically it is an important result as it allows β to be removed from the problem.

As in the two-dimensional case, it is also possible to derive a second consistency condition. First, we note that the integral term in equation (3) vanishes identically when integrated with respect to x from 0 to α. This gives

$$\int_0^\alpha \frac{T''(x)}{2}\left[\frac{1}{2}\log T(x) + \log\left(\frac{\epsilon^2}{4\pi x(\alpha - x)}\right)dx\right] = \pi\alpha - \int_1^\alpha \frac{\beta^2}{16\pi}[T^2(1) - T^2(x)]\, dx. \tag{5}$$

As in the two-dimensional case, (5) will prove to be an invaluable check on any numerical results produced.

2.2. Numerical schemes for solving the integral equation

Before describing a method for the numerical solution of (3), we consider briefly the previous work that has taken place, and point out some of the particular difficulties posed by (3). First, we note that methods in the spirit of those that have proved so successful in two-dimensional cases (see, e.g. O'Malley et al., 1991) are not possible here. In two-dimensional models the kernels that typically arise are of Cauchy type, and may therefore be inverted using standard techniques. Subsequent integrations may then be performed to remove all derivatives and singular integrations from the problem, making the equations

much easier to deal with numerically. In the present case this not possible, as there are no simple inversion formulae for the modulus kernel in (3). We also note that (3) contains second derivatives within the integral term. Any low-order form of approximation (for example, one that employs piecewise constant, linear or quadratic basis functions) is thus doomed to failure as the integral term will inevitably vanish.

Although there is very little literature concerning the numerical solution of integral equations such as (3), problems with certain similarities to (3) have been considered before. Bliss (1982) analyses the flow through a single slot of finite length L, typical width a and planform $t(x)$ in a wall separating a uniform free stream and a quiescent fluid at a different static pressure. The motivation of his study was the need to understand the aerodynamic behavior of slots in transonic wind tunnel walls. Under the assumption that the displacement of the free surface is small compared to the slot width, it may be shown that, for subsonic flows when the Mach number M is less than unity, the free surface displacement $S(x)$ satisfies the equation

$$S'(x)\left(\log\left[\frac{L^2}{a^2(1-M^2)}\right] + \log[4x(1-x)] + \frac{\log 16}{t(x)}\right)$$

$$= \pi\left(\frac{\epsilon L}{a}\right)^2 x + \int_0^L \frac{S'(\xi)}{\xi}\,d\xi + \int_0^L \frac{S'(x) - S'(\xi)}{|x - \xi|}\,d\xi . \tag{6}$$

In contrast to our model, the free surface is never required to reattach and the pressure in the slot is uniform – there is no recirculating region.

In spite of the many similarities between (6) and (3), the numerical solution of (6) is much simpler as the unknown function $S(x)$ occurs only in differentiated form, and moreover appears in a linear fashion. The problem may therefore be solved in straightforward manner by using piecewise constant approximations for the derivatives of S. It was found using this method that accurate solutions could be produced in an economical way, and the scheme could also be used to study the similar case of supersonic flow. Similar remarks also apply to the equations for the stretching of a slender, axisymmetric viscous inclusion that were studied by Fitt and Wilmott (1989), though in this case the flow was unsteady and it was necessary to solve an additional evolution equation.

There appears to be very little literature other than that mentioned above concerning equations that possess similarities to (3). Accordingly we proceed below in an *ad hoc* fashion.

3. A numerical method for solving the integral equation

We now propose a method for the numerical solution of the governing integro – differential equation (3). As discussed above, there seems to be little literature concerning numerical methods for nonlinear integro – differential equations with modulus kernels, and it seems most unlikely we will be able to supply numerical convergence proofs for (3), thus an *ad hoc* method will be proposed.

The interval $[0, \alpha]$ is discretized into N equal intervals of length h where $hN = \alpha$, the intervals being bounded by the points $x_0 = 0, x_N = \alpha$. The method may easily be modified to include the case of unequal mesh spacing (so that, for example, mesh points could be clustered near $x = 0$ and $x = \alpha$) but some preliminary experiments showed that this was not necessary. The values of $T(x)$ at the end points of the interval being known, collocation is

used to determine $T(x)$ at the $N - 1$ interior points of the interval. Because of the second derivatives that appear in the integral term of (3), $T(x)$ is approximated using cubic splines. Writing $T(x_k) = T_k$, we approximate $T(x)$ in the interval $[x_k, x_{k+1}]$ by

$$T(x) = T_k(x) = \frac{1}{6h}[M_k(x_{k+1} - x)^3 + M_{k+1}(x - x_k)^3 + (x_{k+1} - x)(6T_k - h^2 M_k)$$
$$+ (x - x_k)(6T_{k+1} - h^2 M_{k+1})]$$

so that

$$T_k'(x) = \frac{1}{6h}[3(M_{k+1}(x - x_k)^2 - M_k(x - x_{k+1})^2) - 6(T_k - T_{k+1}) + h^2(M_k - M_{k+1})]$$

$$T_k''(x) = \frac{1}{h}[-M_k(x - x_{k+1}) + M_{k+1}(x - x_k)] .$$

The spline coefficients M_k $(k = 0, 1, \ldots, N)$ are chosen in the normal way to ensure that the approximation to $T(x)$ has continuous first and second derivatives, and additionally to ensure that two out of the four conditions $T'(0) = T'(\alpha) = T''(0) = T''(\alpha) = 0$ are satisfied. The spline equations are therefore given by

$$\begin{cases} 2M_0 + M_1 = 6(T_1 - T_0)/h^2 & (T'(0) = 0) \\ M_0 = 0 & (T''(0) = 0) \end{cases}$$

$$M_{k-1} + 4M_k + M_{k+1} = \frac{6}{h^2}(T_{k+1} - 2T_k + T_{k-1}) \quad (k = 1, 2, \ldots, N - 1) \tag{7}$$

$$\begin{cases} M_{N-1} + 2M_N = 6(T_{N-1} - T_N)/h^2 & (T'(\alpha) = 0) \\ M_N = 0 & (T''(\alpha) = 0) . \end{cases}$$

The remaining $N - 1$ equations are given by collocation, and an additional advantage of the spline representation is that the integral term may now be evaluated analytically. After some work we find that, evaluated at the collocation point x_j, the integral term in (3) is given by

$$-\frac{1}{2} \sum_{k=0}^{N-1} I_{jk}$$

where

$$I_{jk} = \begin{cases} (M_{k+1} - M_k) + Q_{jk} \log\left(\frac{j - k - 1}{j - k}\right) & (j < k) \\ M_{k+1} - M_k & (j = k) \\ M_k - M_{k+1} & (j = k + 1) \\ (M_k - M_{k+1}) + Q_{jk} \log\left(\frac{j - k}{j - k - 1}\right) & (j > k + 1) \end{cases}$$

and

$$Q_{jk} = (k - j + 1)M_k - (k - j)M_{k+1} - M_j .$$

Discretizing the remaining terms in (3) at $x = x_j$ in the obvious manner, we find that the $N - 1$ collocation equations that close the system are

$$-\sum_{k=0}^{N-1} \frac{I_{jk}}{2} + \frac{M_j}{2} \log\left[\frac{\epsilon^2 T_j}{4\pi(\alpha - x_j)x_j}\right] + \frac{(6(T_{j+1} - T_j) - h^2(M_{j+1} + 2M_j))^2}{144 h^2 T_j}$$

$$= \begin{cases} \pi & (0 \leq x_j \leq 1) \\ \pi - \beta^2 (T^2(1) - T^2(x_j))/16\pi & (1 \leq x_j \leq \alpha) \end{cases} \quad (j = 1, \ldots, N-1) \qquad (8)$$

where, from the consistency condition discussed above, β is given by (4).

Clearly there are many possible ways to proceed; one possibility is to guess an initial profile for $T(x)$, generate the spline coefficients by solving the linear equations (7), and then solve (8) to produce new values for the T_n, proceeding thereafter by iteration until a complete solution is determined. Numerical experiments show however that this tends to be an ill-conditioned procedure and extremely severe relaxation has to be employed in order to obtain a solution even for a low number of computational points. Another attractive possibility is to treat the equations (8) as linear equations for the spline coefficients, and consider (7) as equations for the T_j. Unfortunately however this stratagem suffers from similar defects. After much experimentation, it has emerged that a superior method is to solve all of the equations simultaneously, ignoring the fact that some are in fact linear and treating the whole system as a set of non-linear equations.

Treating the $2N$ equations (7) and (8) as a system of non-linear equations, the Powell (1970) hybrid method was used to determine a solution. This method is essentially an extension of the well-known Levenburg–Marquardt scheme in which, to solve $f(x) = 0$, successive updates $x^{(i)}$ of the solution are calculated according to a rule of the type

$$x^{(i+1)} = x^{(i)} + (J^T(x_j)J(x_j) + \lambda_j I)^{-1} J^T(x_j)f(x_j)$$

where J is the Jacobian and the λ_j are to be chosen. Space does not permit a fuller explanation of the method, but it combines some of the best features of both Newton's method and the method of steepest descents, whilst using approximate values for the Jacobian in order to preserve economy. The method is easily available in the form of the NAG library routine C05NBF.

4. Numerical results and discussion

The method described above was coded in FORTRAN 77 using DOUBLE PRECISION, running on a SUN SPARC-2. In all the cases described below, the method converged quickly. The method as described above also provides for some additional checks to determine whether or not the current value of α is the correct one; firstly the two (either first or second) derivative conditions that have *not* been imposed may be examined, and secondly we may examine the consistency condition (5) to see whether it is satisfied. In the cases described below, library routines were used to calculate the integrals appearing in (5).

4.1. A numerical test case

In order to test the numerical method, calculations were first carried out using a test case. Although realistic test cases are hard to construct, by ignoring the right-hand side of (3) it is

possible to test the numerical scheme on a problem that shares almost all of the characteristics of the original one. It may easily be checked that, if the right-hand side is replaced by

$$
\frac{9x^4q^2(\beta + 4x^2 - 5x\alpha)^2}{\alpha^5(T(0)\alpha^5 + T(\alpha)x^3\beta - x^3\beta T(0))} - \frac{5q(-44x^3 + 66\alpha x^2 - 24x\alpha^2 + \alpha^3)}{\alpha^5}
$$

$$
+ 30\frac{qx(2x^2 - 3\alpha x + \alpha^2)}{\alpha^5}\log\left[\frac{\epsilon^2\left(T(0) + \frac{qx^3\beta}{\alpha^5}\right)}{4\pi x(\alpha - x)}\right]
$$

where

$$
q = T(\alpha) - T(0), \qquad \beta = 10\alpha^2 - 15\alpha x + 6x^2
$$

then the solution to the problem is given (for arbitrary $\alpha > 1$) by

$$
T(x) = T(0) + \frac{qx^3\beta}{\alpha^5}.
$$

For this solution both the first and second derivatives are zero at both ends of the range. The problem was solved using the method described above, for a variety of conditions and for different numbers of mesh points. Typical results are given in the tables below; in Table 1 zero first derivatives were forced at each end, whilst in the second set of results (Table 2) the second derivatives were set to zero at the ends of the range. In both cases the parameter values $\epsilon = 1/100$, $\alpha = 5$, $T(0) = 5$ and $T(\alpha) = 1$ were used.

A number of conclusions may be drawn from the test cases; in all cases the results are clearly very satisfactory, with accurate values being produced for the variable $T(x)$ even with only a very few collocation points. The results also show that, as might be expected, in general, it is better to prescribe the second derivatives to be zero at the ends of the interval. Some further experiments were carried out with a larger number of mesh points; as is commonly observed in spline and interpolation methods, it was found that when the number of knots is very large there was no significant improvement in the results. Accordingly it was

Table 1. Results for test case with derivatives zero at cavity ends

x	$N = 5$	$N = 10$	$N = 20$	$N = 50$	$N = 100$	EXACT
0.0	5.000	5.000	5.000	5.000	5.000	5.000
0.5		4.962	4.965	4.966	4.966	4.966
1.0	4.745	4.763	4.768	4.768	4.768	4.768
1.5		4.344	4.347	4.348	4.348	4.348
2.0	3.719	3.729	3.730	3.730	3.730	3.730
2.5		3.002	3.001	3.000	3.000	3.000
3.0	2.290	2.275	2.271	2.270	2.270	2.270
3.5		1.659	1.653	1.652	1.652	1.652
4.0	1.259	1.239	1.233	1.232	1.232	1.232
4.5		1.039	1.035	1.034	1.034	1.034
5.0	1.000	1.000	1.000	1.000	1.000	1.000
$T''(0)$	$-2.816E - 1$	$-9.852E - 2$	$-2.805E - 2$	$3.701E - 3$	$8.284E - 4$	0.000
$T''(\alpha)$	$2.973E - 1$	$1.152E - 1$	$4.273E - 2$	$8.959E - 3$	$3.740E - 4$	0.000

Table 2. Results for test case with second derivatives zero at cavity ends

x	$N = 5$	$N = 10$	$N = 20$	$N = 50$	$N = 100$	EXACT
0.0	5.000	5.000	5.000	5.000	5.000	5.000
0.5		4.961	4.965	4.966	4.966	4.966
1.0	4.731	4.763	4.768	4.768	4.768	4.768
1.5		4.344	4.347	4.348	4.348	4.348
2.0	3.717	3.729	3.730	3.730	3.730	3.730
2.5		3.002	3.000	3.000	3.000	3.000
3.0	2.295	2.274	2.271	2.270	2.270	2.270
3.5		1.659	1.654	1.652	1.652	1.652
4.0	1.277	1.239	1.233	1.232	1.232	1.232
4.5		1.040	1.035	1.034	1.034	1.034
5.0	1.000	1.000	1.000	1.000	1.000	1.000
$T'(0)$	0.000	0.000	0.000	0.000	0.000	0.000
$T'(\alpha)$	$-1.124\text{E}-1$	$-2.095\text{E}-2$	$-3.510\text{E}-3$	$-2.220\text{E}-4$	$-4.370\text{E}-6$	0.000

decided to use a maximum of 100 knots in the calculations reported below. All of these conclusions were also confirmed by many other test cases that were run but are now shown here for the sake of brevity.

In spite of this encouraging agreement, it is important to realise that it would be unreasonable to expect this level of accuracy when (3) is solved numerically. For the test case, the right-hand side of the equation is not only chosen in what must be regarded as a very special way, but also there is no consistency condition, and in the full problem it is this that guarantees that both $T''(0)$ and $T''(\alpha)$ are zero. Additionally, the asymptotic analysis of Wilmott and Fitt (1992) shows that the details of the local solution are very subtle, and moreover in the limiting case $\log \epsilon \to -\infty$ it is impossible to satisfy the correct second derivative boundary conditions at the ends of the range. Finally, and perhaps most importantly, a solution exists to the test problem for *any* value of α. This contrasts with the full problem, where, once the cavity heights at each end and the small parameter ϵ have been specified, the quantity α is uniquely determined.

4.2. Numerical results for the full problem

In this section, some numerical results for the full problem (3) are discussed. Guided by the test cases and a large number of numerical experiments, all results given below were computed using the version of the scheme where the second derivatives were prescribed to be zero at the end points of the interval.

As discussed above, the quantity α must be determined for each set of data; this involves an iterative process. For a succession of values of α, the slopes at either end of the cavity were examined, as was the accuracy of the consistency condition (5). Typically, for example when the approximate value of α was taken to be smaller than the correct value, the following behaviour was observed. As α was increased, it was found that the slopes at the cavity ends and the difference between the right- and left-hand sides of (5) simultaneously tended to zero, as expected.

Figures 2(a) and 2(b) show numerical results for a typical case, specifically when the values $\epsilon = 1/100$, $T(0) = 6$ and $T(\alpha) = 1$ are used. For the results shown 100 mesh points were used
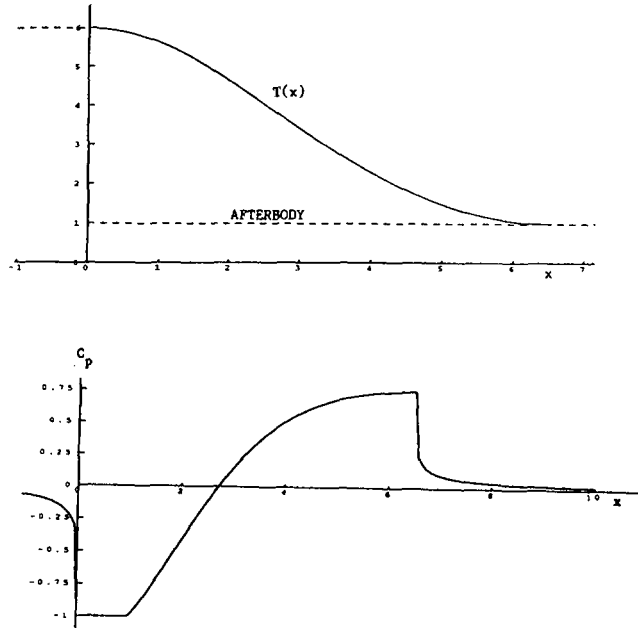
Fig. 2(a). Calculated cavity shape for $T(0) = 6$, $T(\alpha) = 1$ $\epsilon = 1/100$ (afterbody shown dotted). (b) Calculated scaled pressure coefficient $C_p = (p - p_x)/(\frac{1}{2}\rho U_x^2 \epsilon^2)$ for $T(0) = 6$, $T(\alpha) = 1$ $\epsilon = 1/100$.

and α was determined to have a value of 6.50. Figure 2(a) shows the cavity shape whilst Fig. 2(b) shows the pressure coefficient

$$C_p = \frac{p - p_\infty}{\frac{1}{2}\rho U_\infty^2 \epsilon^2} \,.$$

Some studies were also carried out to examine the dependence of the results on the number of mesh points used. Employing 10, 20, 40 and 70 mesh points the computed values for α were 7.44, 7.04, 6.72 and 6.56, respectively, whilst for 200 mesh points the results were virtually indistinguishable from the case shown. Such behaviour is typical of all the cases further considered below.

The method described above relies crucially on the fact that it is possible to determine α for each case by examining the derivatives of $T(x)$ at each end of the cavity. Figure 3 shows
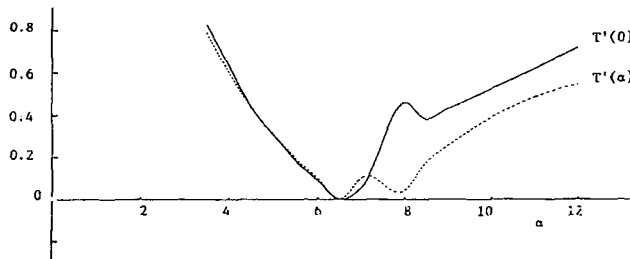

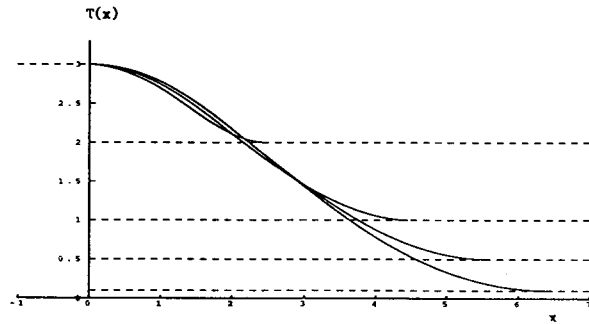*Fig. 3* Cavity slopes at $x = 0$ (solid line) and $x = \alpha$ (dotted) for various values of α.

Fig. 4. Calculated cavity shapes for $T(0) = 3$, $\epsilon = 0.001$ and afterbody heights $2, 1, 0.5$ and 0.1 (afterbodies shown dotted).

calculated values of $T'(0)$ (solid line) and $T'(\alpha)$ (dotted line) plotted against α. It will be observed that both derivatives are *simultaneously* zero when $\alpha = 6.50$. For this value of α the consistency condition (5) is also satisfied to a good degree of approximation.

Figure 4 shows the effect of decreasing the height of the afterbody. As discussed above, we cannot expect to generate solutions with zero curvature when the afterbody height is zero, but for any positive afterbody height the numerical scheme proceeds in an identical fashion to the cases described above. For the calculations shown, 100 mesh points were used and the values $\epsilon = 0.001$, $T(0) = 3$ and $T(\alpha) = 2, 1, 1/2$ and $1/10$ were used, the corresponding calculated values of α being given respectively by $2.45, 4.10, 5.60$ and 6.45. Further numerical experiments have shown that, as might be expected, when the height of the afterbody approaches zero it becomes increasingly difficult to compute solutions that possess zero derivative at the right-hand end of the cavity.

4.3. Numerical solutions for the case $\log \epsilon \rightarrow -\infty$

Although for arbitrary values of ϵ the complexity of (3) precludes closed-form solutions, for very small values of ϵ solutions may be determined for the purposes of comparison. Naively letting $\epsilon \rightarrow 0$ in (3) simply results in the statement that the second derivative of T is zero. Using the numerical method described above it may easily be confirmed that if smaller and smaller values of ϵ are used, then the computed solution rapidly approaches the function $T(x) = T(0) + x(T(\alpha) - T(0))/\alpha$. In this limiting case α is arbitrary and both sides of the consistency condition (5) degenerate to zero. This degenerate exact solution is well reproduced whatever combination of first and second derivatives are prescribed at the ends of the cavity; if the contradictory conditions $T'(0) = 0$ or $T'(\alpha) = 0$ are used then the second derivative of the computed solution merely jumps at the ends of the cavity.

A far more interesting limit occurs when limit $\epsilon \rightarrow 0$ is examined and the natural scalings are carried out as in Section 4 of Wilmott and Fitt (1992). Setting $T(x) = U(x)/(-\log \epsilon)$ and $\beta = -\gamma \log \epsilon$ we have, in the limit $\epsilon \rightarrow 0$,

$$U(x) = D_1 - \frac{\pi x^2}{2} \quad (0 \leq x \leq 1)$$

and for $1 \leq x \leq \alpha$

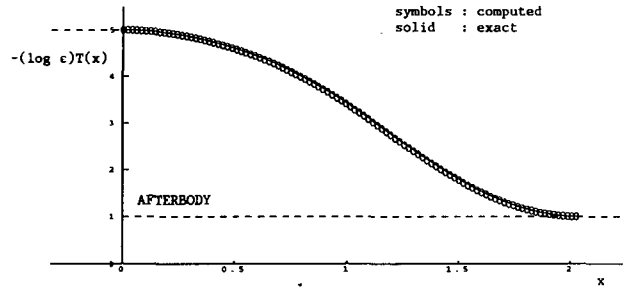$$\alpha - x = \int_{D_2}^{U(x)} \frac{\mathrm{d}\xi}{\sqrt{-P\xi^3 + Q\xi + R}}$$

Fig. 5. Comparison between computed points (symbol) and exact solution (solid line) for the case $\epsilon \to 0$.

where $D_1 = U(0), D_2 = U(\alpha)$ and

$$P = \frac{\gamma^2}{24\pi}, \qquad Q = -2\pi + \frac{\gamma^2 U(1)^2}{8\pi}, \qquad R = 2\pi U(\alpha) - \frac{\gamma^2}{8\pi}\left(U(1)^2 U(\alpha) - \frac{U(\alpha)^3}{3}\right).$$

For a given D_1 and D_2 continuity of U and its first derivative at $x = 1$ then further require

$$\alpha - 1 = \int_{D_2}^{D_1 - \pi/2} \frac{d\xi}{\sqrt{-P\xi^3 + Q\xi + R}} \tag{9}$$

and

$$D_2 - D_1 = \frac{\gamma^2}{16\pi^2}\left(D_2(D_1 - \pi/2)^2 - \frac{1}{3}D_2^3 - \frac{2}{3}(D_1 - \pi/2)^3\right)$$

so that α may be determined.

Figure 5 shows a comparison between the exact solution described above and numerical calculations carried out with 100 points using the values $D_1 = 5, D_2 = 1$ and $\epsilon = 10^{-100}$. For this case it is found from (9) that $\alpha \simeq 2.0488$. In contrast to the cases discussed above, the first derivatives of T were prescribed to be zero at the cavity ends; in this limiting case the (non-zero) second derivatives are given by

$$U''(0) = -\pi, \qquad U''(\alpha) = -\pi + \frac{\gamma^2}{16\pi}((D_1 - \pi/2)^2 - D_2^2) \tag{10}$$

A value for α was therefore determined by minimising the difference between (10) and the computed values of the second derivatives at the cavity ends. The result a calculated value of $\alpha = 2.03$. In Fig. 5 the exact solution is shown using a solid line whilst the computed points are denoted by symbols. The agreement is clearly extremely satisfactory, and provides further evidence of the success of the numerical method.

5. Conclusions

A numerical method has been developed for the solution of a nonlinear singular integro-differential equation. The method relies on the approximation of the unknown function using cubic splines, and collocation at the interior points of the computational region.

Although the inherent non-linearity of the problem means that numerical convergence proofs are not available, by considering test cases and properties of the computed solution for general cases, it is possible to have a large amount of confidence that the scheme is, indeed, computing the correct solution to the equation. The results have implications for models of flow past slender axisymmetric bodies; in particular the length of the cavity for such flows may be computed.

Acknowledgements

References

1. P. Wilmott and A.D. Fitt, A composite cavity model for axisymmetric high Reynolds number separated flow I: Modelling and analysis. *J. Engng. Math.* 26 (1992) 539–555.
2. S. Childress, Solutions of Euler's Equations containing finite Eddies. *Phys. Fluids* 9 (1966) 860–872.
3. K. O'Malley, A.D. Fitt, T.V. Jones, J.R. Ockendon and P. Wilmott, Models for High-Reynolds-Number Flow down a Step. *J. Fluid Mech.* 222 (1991) 139–155.
4. A.D. Fitt, J.R. Ockendon and T.V. Jones, Aerodynamics of slot-film cooling: theory and experiment, *J. Fluid Mech.* 160 (1985) 15–27.
5. M.J.M. Hill, On a Spherical Vortex. *Phil. Trans. R. Soc. London. A* 185 (1894) 213–245.
6. G.K. Batchelor, On steady laminar flow with closed streamlines at large Reynolds number. *J. Fluid Mech.* 1 (1955) 177–190.
7. D.B. Bliss, Aerodynamic Behaviour of a Slender Slot in a Wind Tunnel Wall. *AIAA J.* 20 (1982) 1244–1252.
8. A.D. Fitt and P. Wilmott, The stretching of a slender, axisymmetric, viscous inclusion – part II: numerical solution and results. *SIAM J. Appl. Math.* 49 (1989) 1617–1634.
9. M.J.D. Powell, (1970) A hybrid method for nonlinear equations. In: P. Rabinowitz (ed), *Numerical Methods for Non-linear Algebraic Equations* Gordon & Breach, London, (1970) 87–114.